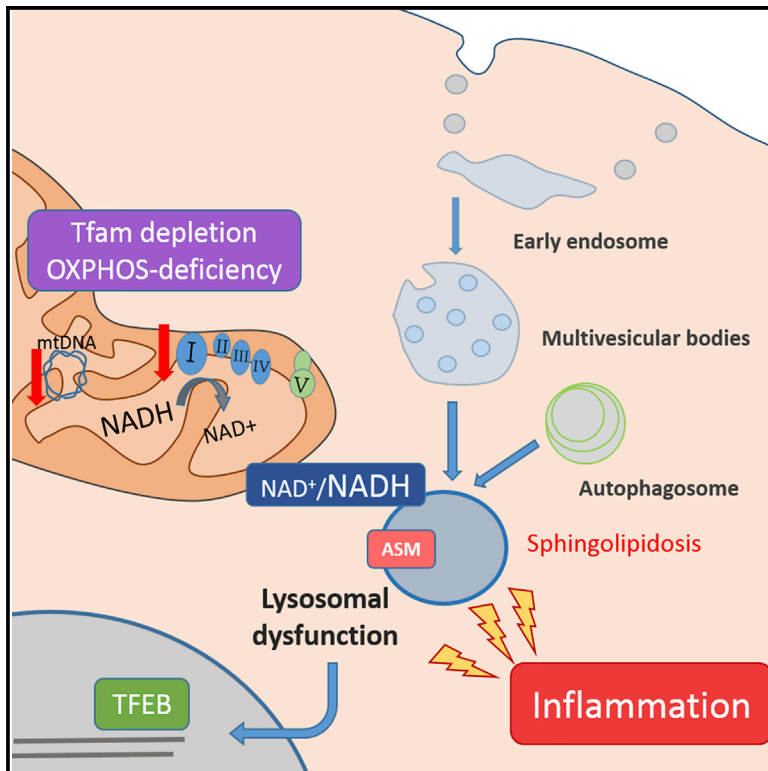


Cell Metabolism

Mitochondrial Respiration Controls Lysosomal Function during Inflammatory T Cell Responses

Graphical Abstract



Authors

Francesc Baixauli, Rebeca Acín-Pérez, Carolina Villarroya-Beltrí, ..., Juan Miguel Redondo, Jose Antonio Enríquez, Maria Mittelbrunn

Correspondence

mmittelbrunn@externo.cnic.es

In Brief

Baixauli et al. show a critical role for mitochondria in the regulation of T cell inflammatory responses by controlling lysosome function. Abnormal endolysosomal function and sphingomyelin accumulation in respiration-impaired cells link mitochondrial dysfunction to lysosomal storage disorders and exacerbated inflammatory responses.

Highlights

- Mitochondrial dysfunction causes lysosomal storage disorder and sphingolipidosis
- Respiration-impaired cells increase lysosomal compartment through TFEB
- Mitochondrial control of lysosome function restrains inflammatory T cell responses
- Restoration of NAD⁺ levels improves lysosome function and inflammatory responses

Mitochondrial Respiration Controls Lysosomal Function during Inflammatory T Cell Responses

Francesc Baixauli,^{1,2} Rebeca Acín-Pérez,³ Carolina Villarroya-Beltrí,^{1,2} Carla Mazzeo,⁴ Norman Nuñez-Andrade,^{1,2} Enrique Gabandé-Rodríguez,⁵ Maria Dolores Ledesma,⁵ Alberto Blázquez,^{6,7} Miguel Angel Martin,^{6,7} Juan Manuel Falcón-Pérez,^{8,9} Juan Miguel Redondo,¹ Jose Antonio Enríquez,³ and Maria Mittelbrunn^{1,*}

¹Signaling and Inflammation Program, Centro Nacional Investigaciones Cardiovasculares Carlos III (CNIC), Madrid 28029, Spain

²Servicio de Inmunología, Instituto Investigación Sanitaria Princesa, Madrid 28006, Spain

³Cardiovascular Metabolism Program, Centro Nacional Investigaciones Cardiovasculares Carlos III (CNIC), Madrid 28029, Spain

⁴Department of Immunology, IIS-Fundación Jiménez Díaz, Madrid 28040, Spain

⁵Department of Molecular Neurobiology, Centro de Biología Molecular Severo Ochoa (CSIC-UAM), Madrid 28049, Spain

⁶Instituto de Investigación Hospital Universitario 12 de Octubre, Madrid 28041, Spain

⁷Centro de Investigación Biomédica en Red de Enfermedades Raras (CIBERER), Madrid 28029, Spain

⁸CIC bioGUNE, CIBERehd, Derio 48160, Spain

⁹IKERBASQUE Research Foundation, Bilbao 48011, Spain

*Correspondence: mmittelbrunn@externo.cnic.es

<http://dx.doi.org/10.1016/j.cmet.2015.07.020>

SUMMARY

The endolysosomal system is critical for the maintenance of cellular homeostasis. However, how endolysosomal compartment is regulated by mitochondrial function is largely unknown. We have generated a mouse model with defective mitochondrial function in CD4⁺ T lymphocytes by genetic deletion of the mitochondrial transcription factor A (Tfam). Mitochondrial respiration deficiency impairs lysosome function, promotes p62 and sphingomyelin accumulation, and disrupts endolysosomal trafficking pathways and autophagy, thus linking a primary mitochondrial dysfunction to a lysosomal storage disorder. The impaired lysosome function in Tfam-deficient cells subverts T cell differentiation toward proinflammatory subsets and exacerbates the *in vivo* inflammatory response. Restoration of NAD⁺ levels improves lysosome function and corrects the inflammatory defects in Tfam-deficient T cells. Our results uncover a mechanism by which mitochondria regulate lysosome function to preserve T cell differentiation and effector functions, and identify strategies for intervention in mitochondrial-related diseases.

INTRODUCTION

Mitochondria are multifunctional organelles that integrate cell metabolism by regulating important anabolic and catabolic pathways. Mitochondria integrate their diverse functions through multiple pathways that ultimately converge on proper function of the respiratory complexes of the electron transport chain (Friedman and Nunnari, 2014). The subunits of these mitochondrial complexes are encoded by both nuclear and mitochondrial DNA (mtDNA), and a correct balance among them is critical to maintaining the function of the electron transport chain, and

is associated with organismal lifespan (Gomes et al., 2013; Houtkooper et al., 2013). The mitochondrial transcription factor A (Tfam) is the most abundant mtDNA-associated protein in mammalian cells, and its expression controls mtDNA copy number in cells, making it an essential player in the maintenance, transcription, and replication of mtDNA (Ekstrand et al., 2004; Larsson et al., 1998). Global deletion of Tfam is embryonically lethal, but tissue-specific ablation of this factor disrupts respiratory chain function in selected cell populations and generates a variety of alterations that recapitulate important phenotypes of human mitochondrial diseases (Vernochet et al., 2012; Viader et al., 2013).

Mitochondria are dynamic organelles that modify their distribution, structure, and function in response to changing circumstances such as oxygen availability or stress (Acín-Pérez et al., 2014; Detmer and Chan, 2007; Lapuente-Brun et al., 2013). Moreover, the crosstalk of mitochondria with other intracellular organelles is crucial during cell adaptation to stresses and for the preservation of organelle functionality (Rowland and Voeltz, 2012). Contacts between mitochondria and the endoplasmic reticulum form critical hubs implicated in the regulation of mitochondrial fission, calcium homeostasis, ATP production, apoptosis, and lipid metabolism, and deregulation of these contacts can lead to disease (Arruda et al., 2014). In addition, mitochondrial contacts with the lysosome-related vacuole in yeast (Elbaz-Alon et al., 2014; Hönscher et al., 2014) and with melanosomes in melanocytes (Daniele et al., 2014) have been shown to modulate lipid homeostasis and organelle function. Defining the intricate communication of mitochondria with other intracellular organelles is thus critical for understanding essential physiological processes and how their dysfunction might contribute to the development of human disease.

The endolysosomal system is a dynamic membrane compartment critical to the maintenance of cellular homeostasis. Endosomes, multivesicular bodies, and lysosomes regulate signaling, secretion, and the recycling and degradation of protein and lipid cellular components. Lysosomes are critical organelles with degradative and recycling functions, but also mediate other fundamental processes such as plasma membrane repair,

signaling, and regulation of lipid metabolism (Settembre et al., 2013b). Lysosome biogenesis and function are subjected to transcriptional regulation by the transcription factor EB (TFEB), which allows adaptation of lysosomal function to different physiological conditions (Medina et al., 2015). Alterations to lysosome function and endolysosomal trafficking pathways are mostly found in lysosomal storage disorders (LSDs). LSDs are caused either by deficiency of lysosomal proteins or by changes in non-lysosomal proteins that result in the accumulation of undegraded substrates in lysosomes and abnormal storage of lipids such as sphingomyelins (SMs), triacylglycerides (TAGs), glycosphingolipids, or sphingosines (Futerman and van Meer, 2004). Remarkably, lysosomal dysfunction in Gaucher disease blocks mitochondrial turnover by mitophagy (Osellame et al., 2013), thus connecting the lysosome degradation capacity to the maintenance of a healthy mitochondrial repertoire. Whether mitochondria regulate the biogenesis and function of the endolysosomal compartment is still unknown.

During adaptive immune responses, naive CD4⁺ T cells that encounter a foreign antigen must reprogram their metabolism to meet the costly biosynthetic and bioenergetic demands of cellular activation, proliferation, and effector function (Pearce et al., 2013). T cells reorient their metabolism toward aerobic glycolysis. Although less efficient at ATP synthesis, glycolysis generates intermediate metabolites that support biosynthetic pathways for effector functions, including cytokine production (Chang et al., 2013). Because of the glycolytic nature of T lymphocyte metabolism, the role of mitochondria in T cell function has been traditionally neglected. However, accumulating evidence indicates that T cell effector functions require mitochondrial oxygen consumption, ATP, and ROS (Weinberg et al., 2015).

To investigate the mechanisms by which mitochondria influence T cell responses and ultimately affect immune disease progression, we have generated a mouse model in which mitochondrial function is specifically disrupted in the adaptive immune system by targeting *Tfam* in CD4⁺ T cells. *Tfam*-deficient cells have below-normal levels of mtDNA, diminished mitochondrial respiration, and a metabolic signature characterized by increased anaerobic glycolysis and impaired fatty acid β -oxidation. Respiration-impaired cells show reduced lysosomal calcium mobilization and impaired lysosomal degradation capacity revealed by p62 and SM accumulation, defects that cells try to compensate by inducing lysosome biogenesis through the TFEB. The impaired lysosome function in *Tfam*-deficient cells subverts T cell differentiation toward proinflammatory subsets and exacerbates the in vivo inflammatory response. Improvement of lysosome function by restoration of NAD⁺/NADH balance through NAD⁺ precursors corrected inflammatory defects in *Tfam*-deficient T cells. These data reveal a mechanism by which mitochondria regulate lysosome function to preserve T cell differentiation and effector functions.

RESULTS

Tfam Depletion Impairs Respiratory-Chain Function in T Cells

To investigate the involvement of mitochondria in the regulation of endolysosomal function and T cell responses, we generated a

mouse model of mitochondrial dysfunction by specifically deleting *Tfam* in CD4⁺ T cells. This was achieved by crossing mice with loxP-flanked *Tfam* alleles (*Tfam*^{fl/fl}) with CD4-Cre mice. Consistent with gene deletion in the early stages of T cell development, *Tfam* deletion efficiently decreased the mRNA of *Tfam* in CD4⁺ and in CD8⁺ T naive lymphocytes (see Figures S1A and S1B). CD4Cre^{+/wt}*Tfam*^{fl/fl} mice (herein *Tfam*^{-/-} mice) developed normally and showed similar frequency of CD4 and CD8 single-positive and double-positive thymocytes to their control littermates (Figure 1A), indicating that *Tfam* is not required during early T cell development. *Tfam*^{-/-} mice presented slightly lower percentages of CD4⁺ and CD8⁺ T cells in the spleen and peripheral lymph nodes (Figure 1B), but had similar numbers of splenocytes, B cells and dendritic cells to littermate CD4Cre^{wt/wt}*Tfam*^{fl/fl} controls (herein WT mice) (Figure S1C).

Naive *Tfam*^{-/-} CD4⁺ T cells expressed comparable levels of T cell surface markers to WT cells and responded normally to in vitro differentiation toward T lymphoblasts, adopting a polarized morphology (Figures 1C and 1D). The levels of *Tfam* were suppressed throughout lymphoblast differentiation, excluding the selection of *Tfam*-positive cells during in vitro expansion (Figures 1E and 1F). Consistent with the close relationship between levels of *Tfam* and mtDNA, lack of *Tfam* induced a severe decrease in mtDNA content, both in *Tfam*^{-/-} CD4⁺ T lymphoblasts and in human Jurkat T cells stably transfected with *Tfam* short hairpin RNAs (sh*Tfam*) (Figures 1G and S1D). *Tfam* deficiency reduced the mRNA expression of mtDNA-encoded subunits of mitochondrial complexes I, III, IV, and V, whereas nuclear-encoded subunits were not affected (Figure 1H). Consistently, the protein levels of complexes I and IV, which include mtDNA-encoded subunits, were below normal, whereas the nuclear-encoded complex II was unaffected (Figure 1I).

In response to these respiratory-chain alterations, *Tfam*-deficient cells increased mitochondrial mass (Figure 2A). However, electron microscopy analysis revealed severely aberrant mitochondrial morphology in *Tfam*^{-/-} CD4⁺ T cells, impaired cristae organization, and loss of mitochondrial electron density (Figure 2B), consistent with a mitochondrial dysfunction caused by *Tfam* depletion.

Blue native gel electrophoresis (BNGE) of extracts from *Tfam*-silenced cells revealed severe loss of complexes I and III, but not II, and associated alterations in mitochondrial supercomplex assembly (Figure 2C). Accordingly, *Tfam*-depleted cells showed stronger impairment of electron transport from NADH (complexes I+III) than from FADH₂ (complexes II+III) (Figure 2D), demonstrating an imbalance in the NAD⁺/NADH ratio in respiratory-chain impaired cells. Connected with the reduced electron transport chain function, *Tfam*-deficient T cells also had below-normal content of mitochondrial reactive oxygen species (ROS) (Figure 2E), reduced mitochondrial ATP generation (Figure 2F), and impaired survival in galactose medium (Figure S1E). Inhibition of electron transport chain function by oligomycin treatment caused a transient hyperpolarization in WT cells, where mitochondrial membrane potential is maintained by OXPHOS function. In contrast, oligomycin treatment did not increase mitochondrial membrane potential in *Tfam*^{-/-} cells, in agreement with absence of mtDNA-encoded F₀ subunits (Appleby et al., 1999; Buchet and Godinot, 1998) (Figure S1F). The maintenance

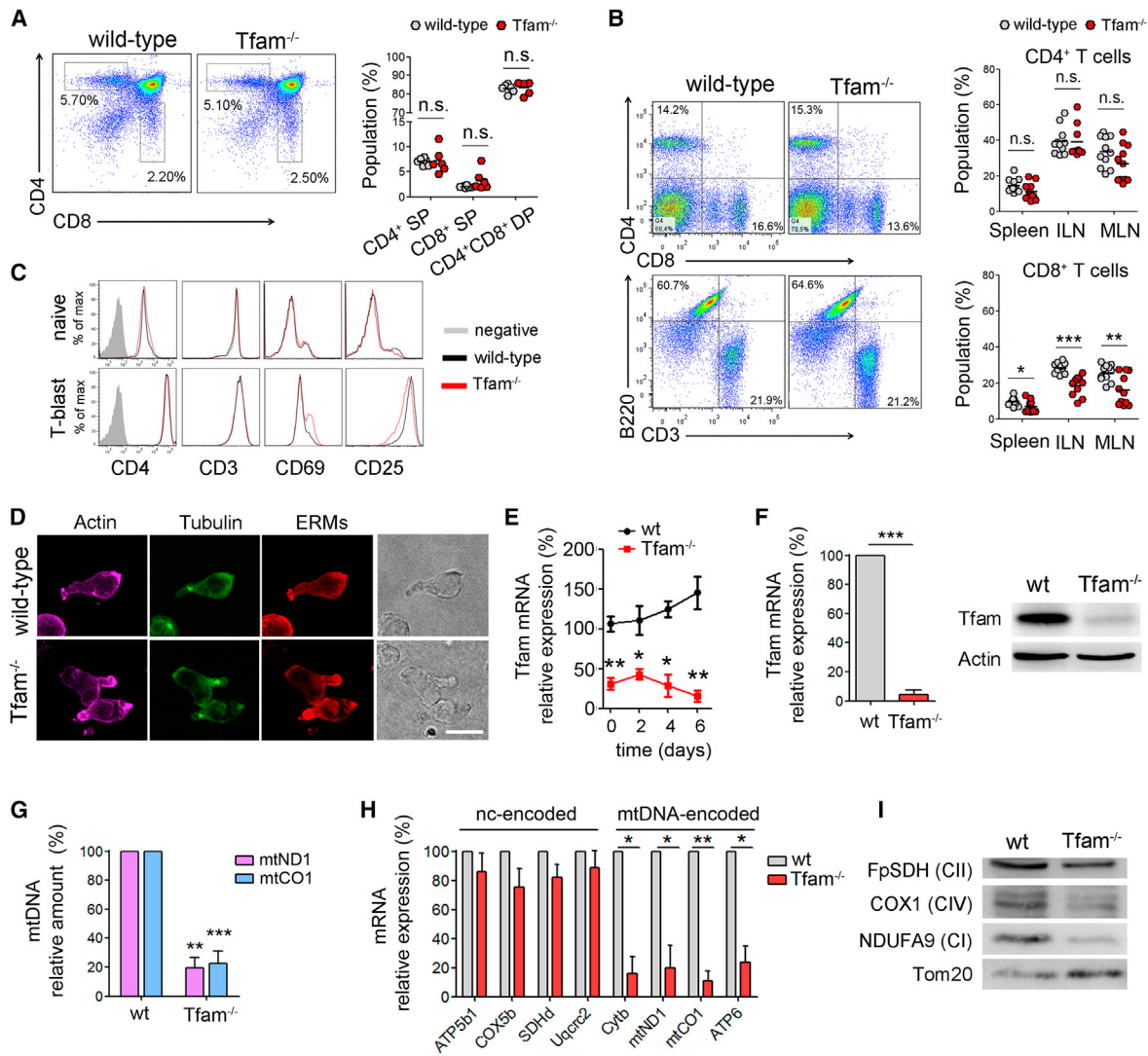


Figure 1. Tfam Depletion Induces Severe mtDNA Deficiency in T Cells

(A) Dot plots show CD4 and CD8 expression in thymocytes from WT and *Tfam*^{-/-} mice. Right, percentage of CD4 and CD8 single-positive (SP), and CD4/CD8 double-positive (DP) cells.
 (B) Dot plots show CD4 and CD8 T cells, and CD3 and B220 cells from the spleens. Right, percentages of CD4 and CD8 cells in the spleen, inguinal (ILN), and mesenteric lymph nodes (MLN) (n = 11).
 (C) Expression of cell-surface markers in naive CD4 T cells and T-lymphoblasts differentiated with ConA (48 hr) and IL-2 (4 days).
 (D) Confocal images show polarization of cytoskeletal components in T lymphoblasts by actin, tubulin, and ERM (ezrin-radixin-moesin) staining. Scale bar, 10 μ m.
 (E) Relative Tfam mRNA levels by RT-PCR in naive CD4 T cells (day 0) and during lymphoblast differentiation.
 (F) Tfam mRNA (left) and protein levels (right) in CD4 T lymphoblasts.
 (G) mtDNA levels (mtCO1 and mtND1) relative to nuclear DNA (SDH) in CD4 T lymphoblasts.
 (H) mRNA levels of mtDNA-encoded and genome-encoded mitochondrial subunits.
 (I) Immunoblot of T lymphoblast mitochondrial proteins. Complex I (CI) was detected with anti-NDUFA9, CII with anti-FpSDH, and CIV with anti-COX1. Tom20 was used as loading control. Data (B and E–H) are means \pm SEM (n > 3); *p < 0.05, **p < 0.01, and ***p < 0.001 (Student's t test).

of mitochondrial membrane potential in mtDNA-depleted cells is thought to require the reverse function of the F1-ATPase and action of the adenine nucleotide carrier (Appleby et al., 1999; Buchet and Godinot, 1998). Despite the effect on electron transport chain function and mitochondrial ATP production, total cellular ATP content in primary CD4⁺ *Tfam*^{-/-} T cells and Jurkat shTfam T cells was comparable with controls (Figures 2G and S1G). In addition, the phosphorylation level of the metabolic sensor

AMP-activated protein kinase (AMPK) did not differ between *Tfam*-deficient and control cells (Figure 2H), indicating that global energy status is not compromised in *Tfam*-depleted cells.

We then analyzed the metabolic consequences of *Tfam* deletion on CD4⁺ T cells by flux analysis. In activated CD4⁺ T cells, we measured the extracellular acidification rate (ECAR), as an index of lactate production and glycolysis, and the oxygen consumption rate (OCR) as an indicator of mitochondrial oxidative

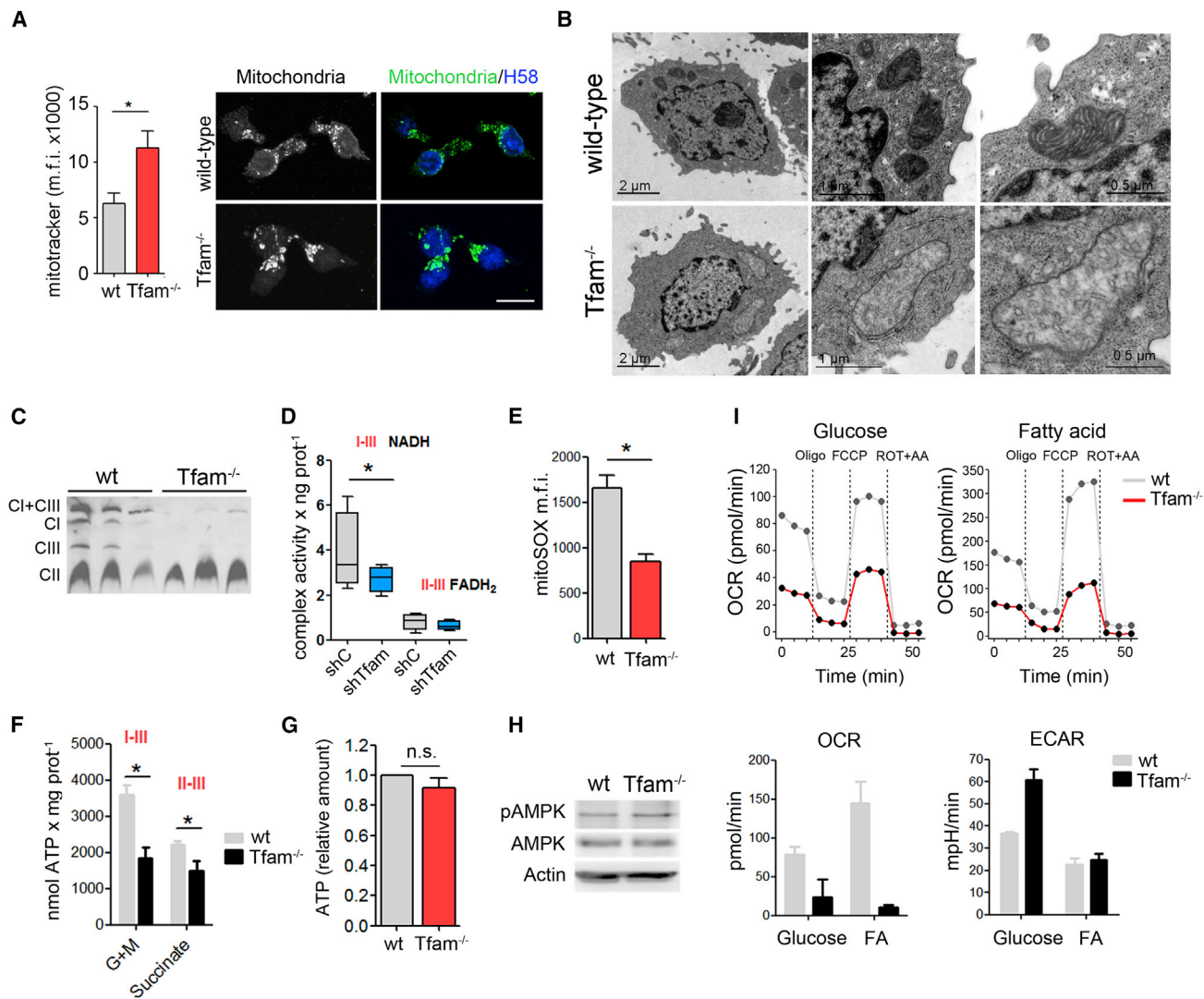


Figure 2. Tfam Ablation Induces OXPHOS Deficiency in T Cells

(A) Left, flow cytometry analysis of Mitotracker staining. Right, confocal images of mitochondria (anti-MnSOD), and nuclei HOECHST58 (H58, blue) in T lymphoblasts. Scale bar, 10 μm.

(B) Electron microscopy images in T lymphoblasts.

(C) Blue native gel electrophoresis analysis of electron-transport-chain complexes (NDUFA9, FpSDH, and Core1 for complexes I, II, and III, respectively) from three WT and Tfam^{-/-} T cell lysates.

(D) Combined mitochondrial complex activities in Jurkat T cells. Lines extending from the boxes indicate the variability outside the upper and lower quartiles.

(E) Flow cytometry analysis of mROS in T lymphoblasts stained with MitoSOX.

(F) Glutamate- and pyruvate-driven ATP-dependent production in Jurkat T cells.

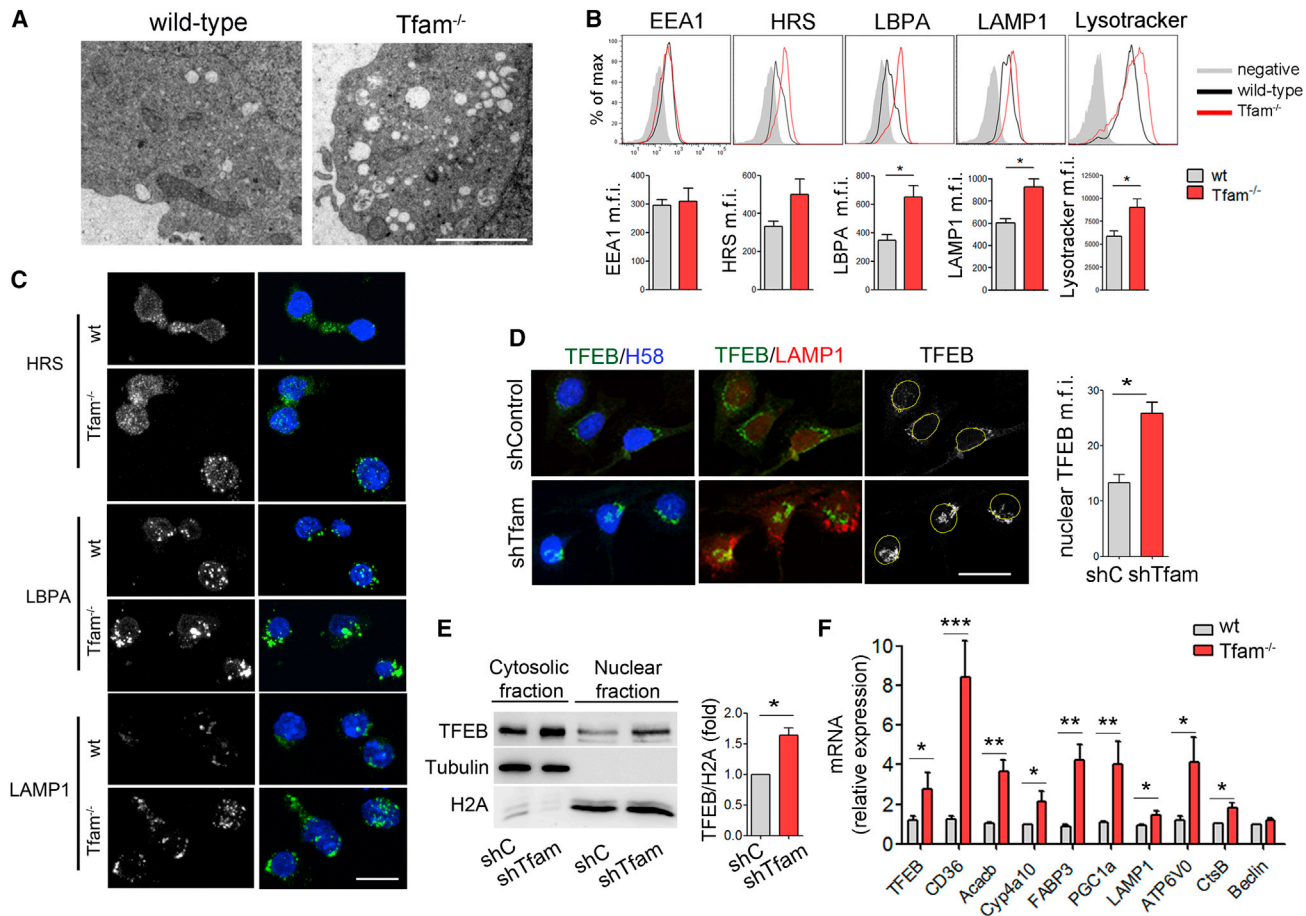
(G) Cellular ATP content in WT and Tfam^{-/-} T cells.

(H) Immunoblot analysis of AMPK phosphorylation at Thr172 in T lymphoblasts. Actin was used as a loading control.

(I) CD3/CD28-activated CD4 T cells fed either with glucose or palmitate (FA) for 2 hr and oxygen consumption rate (OCR) and extracellular acidification rate (ECAR) measured in real time (upper panels). Lower panels show the basal OCR and ECAR from a representative experiment. Data (A and D–G) are means ± SEM (n ≥ 3, *p < 0.05, Student's t test).

phosphorylation (OXPHOS). Upon activation with anti-CD3 and anti-CD28, wild-type T cells used glycolysis and OXPHOS for glucose consumption, as described (Michalek et al., 2011; Pearce et al., 2013). In contrast, Tfam^{-/-} T cells presented a low OCR and an ECAR above WT levels, demonstrating anaerobic glucose utilization (Figure 2I). Additionally, we examined mitochondrial fatty acid β-oxidation (FAO) in respiration-deficient cells.

Naive CD4⁺ T cells were activated over 48 hr and then incubated with fatty acids prior to flux analysis. In these conditions, activated wild-type CD4⁺ T cells showed increased OXPHOS and reduced glycolysis, thus relying on FAO and mitochondrial OXPHOS for energy production. In contrast, Tfam^{-/-} T cells showed reduced OCR, supporting the conclusion that FAO is impaired in respiratory-chain deficient cells (Figure 2I).



Tfam deletion thus promotes loss of mtDNA, OXPHOS deficiency, and compromised mitochondrial function, but has no significant impact on cellular energy status or survival. Additionally, impaired mitochondrial respiration induces a metabolic reprogramming characterized by increased anaerobic glucose consumption and impaired FAO.

Respiration-Impaired Cells Increase Lysosomal Compartment through TFEB

In addition to the profound morphological and functional mitochondrial alterations, electron microscopy studies revealed striking intracellular vesiculation in *Tfam*-deficient cells (Figure 3A). These abnormalities prompted us to explore the role of mitochondria in the abundance and organization of the endolysosomal compartment. By flow cytometry, the early endosome marker EEA1 showed no substantial differences, but expression of the late endosomal markers HRS and lysobisphosphatidic

acid (LBPA) was elevated in respiratory-chain impaired cells (Figure 3B). Immunofluorescence analysis revealed enlargement of late endosomes in *Tfam*^{-/-} cells (Figures 3C). In addition, lysosomes, identified by staining for LAMP1 and Lysotracker, appeared to be more abundant in *Tfam*^{-/-} cells than in wild-types (Figures 3B and 3C), indicating the expansion of the late endosome and lysosome compartment in cells that lack Tfam.

Lysosomal biogenesis is regulated by TFEB, a master regulator of the coordinated lysosomal expression and regulation (CLEAR) gene network (Sardiello et al., 2009). During lysosomal stress or starvation, cytosolic TFEB relocates to the nucleus and activates a transcriptional program aimed at increasing autophagy and lysosomal biogenesis and function (Settembre et al., 2013b). TFEB is also responsible for the transcriptional activation of PGC1 α , which adjusts the content of mitochondrial and peroxisomal enzymes and the expression of components that increase lipid catabolic reactions (Settembre et al., 2013a).

Confocal analysis revealed that TFEB translocates to the nucleus in *Tfam*-depleted cells (Figures 3D and S2A). Nuclear localization of TFEB was confirmed by cell fractionation assays (Figure 3E and S2B) and correlated with upregulated expression of the TFEB target genes LAMP1, ATP6V0, CtsB, FABP3, CD36, Acacb, Cyp4a10, and PGC1 α (Figure 3F), which are involved in lipid uptake, lipid catabolism, and lysosomal and mitochondrial function. These results suggest that the enlarged lysosomal compartment observed in respiration-impaired *Tfam*^{-/-} cells is associated with TFEB activation.

Mitochondrial Dysfunction Promotes Lysosomal Disorder and Sphingolipidosis

To further examine the impact of *Tfam* deficiency on lysosome function, we measured the levels of calcium in lysosomes after inducing its release with bafilomycin-A1 (Lloyd-Evans et al., 2008), a selective inhibitor of the vacuolar-type H⁺ ATPase. Lysosomal calcium mobilization was weaker in *Tfam*-deficient cells (Figure 4A), whereas the subsequent addition of ionomycin, which releases calcium from remaining stores, triggered comparable release in WT and *Tfam*^{-/-} T cells. Measurement with a specific lysosomal pH-sensitive probe indicated reduced pH in lysosomes from respiration-impaired *Tfam*^{-/-} cells (Figure S3A). The activity of the lysosomal endopeptidase cathepsin B was significantly reduced in *Tfam*^{-/-} T cells (Figure 4B), whereas acid phosphatase activity showed no difference (Figure S3B).

SMs and other lipids such as cholesterol, glycosphingolipids and sphingosine accumulate abnormally in LSDs (Futerman and van Meer, 2004). Lipidomic analysis showed that CD4⁺ *Tfam*^{-/-} T cells have an altered lipid profile compared with wild-types, affecting 90 out of 218 lipids analyzed and characterized by elevated levels of several lipid species (Figure 4D). Consistent with the reduced lysosomal degradation capacity, respiration-impaired *Tfam*^{-/-} cells showed a significant accumulation of SMs and TAGs (Figures 4D and S3C). Supporting lysosomal dysfunction and SM accumulation in respiration-impaired cells, *Tfam*^{-/-} T cells showed significantly reduced acid sphingomyelinase (ASM) activity (Figure 4C).

To dissect how mitochondria regulate lysosomal function, we investigated whether cells containing point mutations in mtDNA genes for specific mitochondrial respiratory complexes undergo the same lysosomal calcium defects. Mouse fibroblasts that carry a high load (98%) of a null mutation in the mt-ND6 gene (complex I subunit, CI) showed impaired lysosomal calcium mobilization, upregulation of TFEB target genes, and reduced ASM activity (Figures 4E–4G). Notably, impaired lysosomal calcium mobilization was also detected in fibroblasts from two human patients, one carrying a high load (88%) of a point mutation in the mt-tRNA^{Asn} gene (m.5658T>C), and another carrying a 50% load of a point mutation in the CI subunit mt-ND5 gene (m.13513G>A) (Figure 4H). These results indicate that lysosomal calcium levels are decreased not only by the severe OXPHOS deficiency associated with *Tfam* depletion, but also by point mutations in mtDNA associated with CI dysfunction, both in mice and in human patient samples.

Defects in lipid trafficking and autophagosome-lysosome fusion are commonly observed in sphingolipidoses. The reduced lysosomal calcium and abnormal SM accumulation detected in

respiration-impaired cells prompted us to investigate the ability of lysosomes to fuse with autophagosomes. In cells transfected with the autophagosome marker LC3GFP-RFP, GFP fluorescence is decreased when autophagosomes fuse with lysosomes because it is more sensitive to pH than RFP, which is maintained in acidic compartments. In these experimental settings, control cells showed increased RFP puncta upon induction of autophagy by rapamycin (Figure 4I). In contrast, *Tfam*-deficient cells showed a significant reduction in the number of RFP-positive puncta, indicating impaired autophagosome-lysosome fusion in the absence of *Tfam*. Assessment of mitochondrial degradation by mitophagy upon acute membrane depolarization with CCCP revealed larger parkin-GFP aggregates in *Tfam*-deficient cells than in control cells (Figure S3D), indicating impaired parkin clearance and mitochondrial degradation.

In accordance with impaired autophagic flux, *Tfam*-depleted cells showed increased levels of the lipidated form of LC3 (LC3-II) (Figure S3E). Additionally, flow cytometry, western blot, and confocal analysis showed a significant accumulation of the autophagic substrate p62 in *Tfam*-deficient cells (Figure 4J). Blocking protein synthesis with cycloheximide revealed slower p62 turnover in respiration-impaired cells than in wild-types, suggesting that the accumulation of p62 was caused by impaired lysosomal degradation and not by increased mRNA transcription (Figure 4K).

Cells that lack *Tfam* exhibit lysosomal defects similar to those seen in LSDs: abnormal lipid trafficking, altered calcium mobilization, and defective autophagosome-lysosome fusion. Overall, these results reveal a link between a primary mitochondrial dysfunction and the acquisition of a lysosomal storage disorder.

Tfam Deficiency Exacerbates Inflammatory Responses

We next assessed how these mitochondrial and endolysosomal alterations caused by *Tfam* deficiency affect T cell effector function. Upon T cell activation, *Tfam* expression increased concomitantly with an increase in mtDNA levels (Figures 5A and S4A), suggesting that mitochondrial adaptation to T cell activation requires an increase in mtDNA levels. T cells from wild-type and *Tfam*^{-/-} mice were labeled with the proliferation indicator Cell Violet, stimulated with anti-CD3 and anti-CD28 antibodies, and evaluated by flow cytometry. *Tfam*^{-/-} T cells showed reduced proliferation (Figure 5B). Moreover, upon in vitro cell activation, there was no evidence of higher apoptosis in *Tfam*^{-/-} T cells, as assessed by flow cytometry analysis of annexin V and HOECHST58 staining (Figure S4B). CD4⁺ *Tfam*^{-/-} cells showed similar levels of the activation markers CD69 and CD25 (Figure S4C). Stimulated *Tfam*^{-/-} CD4⁺ T lymphocytes showed increased numbers of IFN- γ - and T-bet-producing cells compared to wild-type cells (Figure 5C). RT-PCR analysis indicated strikingly elevated mRNA expression of the proinflammatory cytokines IFN- γ , IL-6, IL-1 α , and IL-1 β , and increased IFN- γ and IL-6 secretion were detected in the supernatant of *Tfam*^{-/-} T cells (Figures 5D, S4D, and S4E). In contrast, IL-4 mRNA levels and cytokine secretion of IL-4 and IL-10 were below-normal in *Tfam*^{-/-} cells (Figures S4D and S4E). These in vitro data highlight the requirement on mitochondrial function for the fine regulation of T cell responses.

To assess the role of mitochondria in the regulation of the inflammatory function of T cells in vivo, we first examined a model

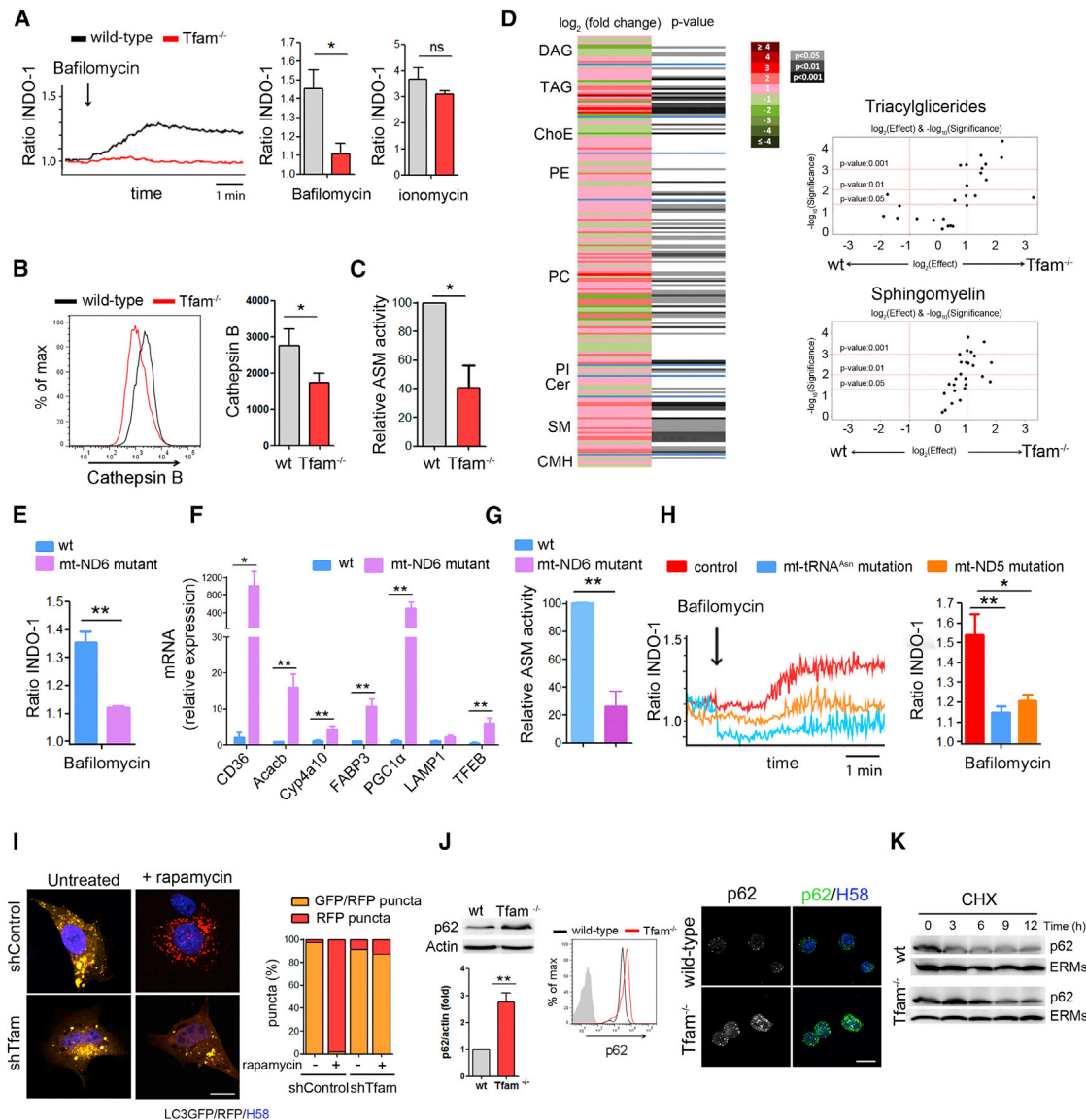


Figure 4. Tfam Controls Lysosomal Function

(A) Lysosomal calcium mobilization in T lymphoblasts loaded with Indo-1, treated with bafilomycin-A1 and detected by flow cytometry. The 340/380 nm ratio is shown. Right, quantification of Indo-1 signal in bafilomycin-A1- or ionomycin-treated cells relative to basal level.

(B) Histograms and quantification of Cathepsin B activity measured by flow cytometry (MagicRed).

(C) Acid sphingomyelinase (ASM) activity in T lymphocytes.

(D) Heatmap represents cell lipidomic signatures of T cells (n = 3). More intense colors indicate larger drops (green) or elevations (red) of the metabolite levels in *Tfam*^{-/-} samples. DAG, diacylglyceride; TAG, triacylglyceride; ChoE, cholesteryl ester; PE, phosphatidylethanolamine; PC, phosphatidylcholine; PI, phosphatidylinositol; Cer, ceramide; SM, sphingomyelin; CMH, monohexosylceramide. Right, volcano plots (\log_{10} [p value] versus \log_2 [fold change]) for the comparison of *Tfam*^{-/-} and WT T cells for the indicated metabolites.

(E) Lysosomal calcium in mt-ND6 Complex I (CI) mutant and WT fibroblasts treated as in (A). Ratio of Indo-1 signal upon bafilomycin-A1 treatment relative to the basal level.

(F) Relative mRNA levels of TFEB and selected target genes assessed by RT-PCR.

(G) ASM activity in WT and mt-ND6 mutant fibroblasts.

(H) Lysosomal calcium in fibroblasts from patients with point mutation in CI subunit mt-ND5 gene (m.13513G>A), point mutation in the mt-tRNA^{Asn} gene (m.5658T>C) or control samples assessed as in A.

(I) Left, confocal images show Oli-Neu transfected with LC3-GFP-RFP treated or not with rapamycin. Right graph, percentage of GFP/RFP puncta (yellow vesicles) and RFP puncta (red vesicles) from at least 100 vesicles in two independent experiments.

(J) Analysis of p62 by western blot, flow cytometry, and confocal immunofluorescence in T lymphoblasts. Chart shows densitometry analysis of p62 by western blot.

(K) Western blot analysis of p62 turnover in cells treated with cycloheximide for the indicated times. ERMs are used as loading control. Data (A–C, E–H, and J) are means \pm SEM, n \geq 3; *p < 0.05 and **p < 0.01 (Student's t test). Scale bars, 10 μ m.

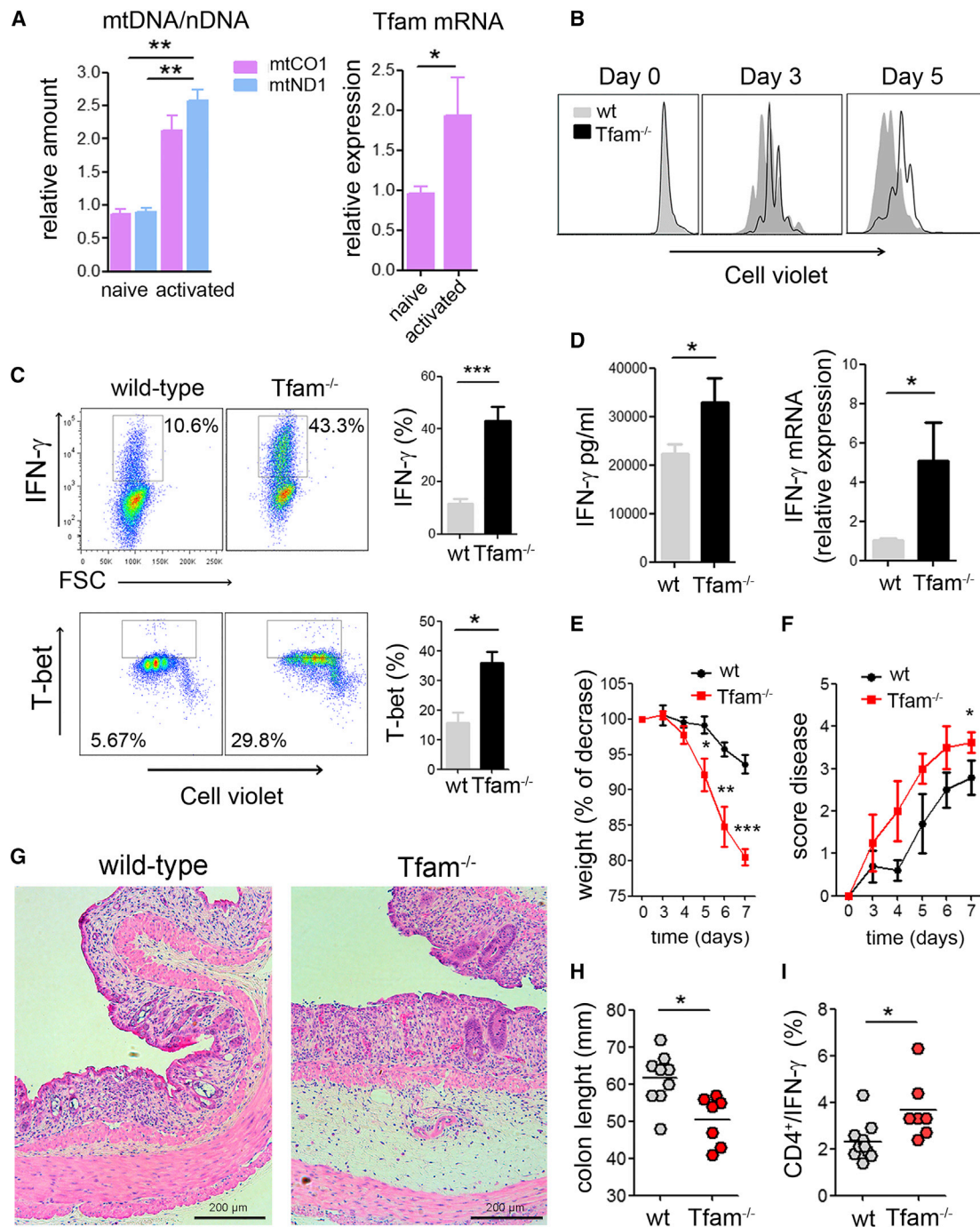


Figure 5. Inhibition of OXPHOS Exacerbates Inflammatory Responses In Vitro and In Vivo

(A) Relative mtDNA and Tfam mRNA levels in naive and CD3/CD28 activated CD4 T cells.

(B) Cell proliferation analysis by Cell Violet dilution of CD4 T cells activated with CD3/CD28.

(C and D) CD4 T cells were activated with CD3/CD28 (6 days), and IFN- γ and T-bet intracellular levels were measured by flow cytometry (C), IFN- γ secretion by ELISA and relative IFN- γ mRNA levels by RT-PCR (D).

(E and F) (E) Weight and (F) disease score were monitored for the indicated times in mice fed with 3% dextran sulfate sodium (DSS) in the drinking water.

(G and H) H&E staining of colon sections (G) and colon length (H) on day 7 after DSS treatment.

(I) IFN- γ -producing CD4 T cells in the mesenteric lymph nodes. Data are means \pm SEM, (A, C, and D, $n \geq 3$) (E-I, seven mice in two independent experiments); * $p < 0.05$ and ** $p < 0.01$, *** $p < 0.001$ (Student's t test).

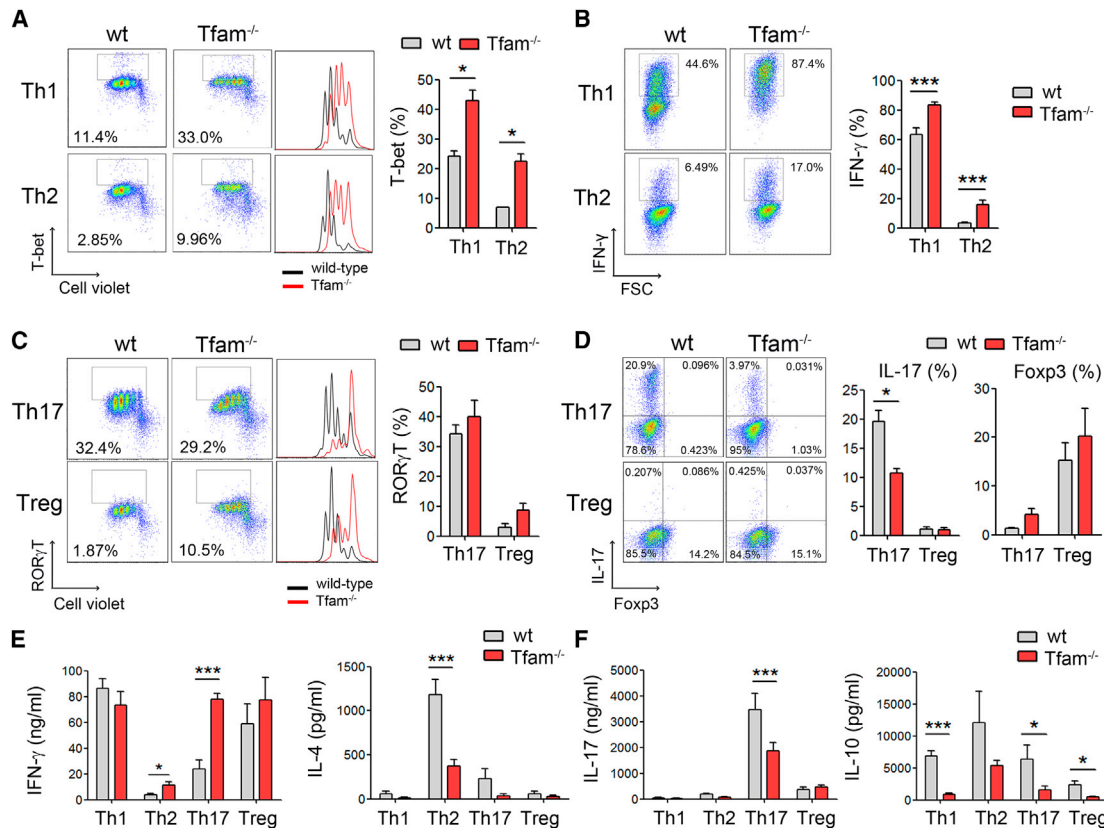


Figure 6. Mitochondrial Dysfunction Subverts T Cell Differentiation toward Th1 Cell Subsets

(A) Cell Violet dilution and T-bet expression in CD4 T cells cultured under Th1 and Th2 conditions over 3 days. Chart shows percentage of T-bet expressing cells (n = 3). (B) Intracellular flow cytometry analysis of IFN- γ -producing cells under Th1 and Th2 conditions over 6 days. Graph, quantification of IFN- γ -producing cells (n = 6). (C) Naive CD4 T cells were cultured under Th17 and Treg conditions over 3 days. Dot plots show ROR γ T-expressing cells and histograms show cell proliferation assessed by Cell Violet dilution. Chart shows percentage of ROR γ T-expressing cells (n = 3). (D) Intracellular flow cytometry analysis of CD4 T cells producing IL-17 and Foxp3. Chart shows percentage of IL-17 and Foxp3-producing cells (n = 6). (E and F) Polarized CD4 T cells at day 6 were cultured in equal numbers in fresh medium followed by activation with PMA/ionomycin for 16 hr. Cytokines were measured by ELISA in the supernatants. Data are means \pm SEM (n \geq 3); *p < 0.05, **p < 0.01, and ***p < 0.001 (Student's t test).

of contact hypersensitivity (CHS), which is mainly mediated by IFN- γ . The specificity of the CHS response is generally defined as the difference between ear swelling responses to a hapten such as oxazolone in naive and sensitized animals. Upon sensitization to oxazolone, *Tfam*^{-/-} mice showed larger increases in ear thickness, lymph node cellularity, and IFN- γ -producing CD4⁺ T lymphocytes (Figure S4F). In addition, we performed a model of DSS-induced colitis, which is driven by Th1 and Th17 cells and suppressed by Treg cells. Wild-type mice and *Tfam*^{-/-} mice were fed with DSS to induce gut damage and trigger disease. *Tfam*^{-/-} mice showed increased disease severity, as reflected by higher weight loss over time, increased disease score, and shorter colon length than WT mice (Figures 5E–5H, S4G, and S4H). Remarkably, *Tfam* deficiency increased the frequency of IFN- γ - and T-bet-expressing CD4⁺ T cells in the mesenteric lymph nodes upon DSS treatment (Figures 5I and S4I). These results indicate that respiration-impaired T cells develop a stronger inflammatory response in vitro and in vivo and support a critical role for mitochondria in the regulation of T cell effector functions during immune responses.

Mitochondrial Dysfunction Deviates T Cell Differentiation toward Proinflammatory Th1 Subsets

To provide further insights into how mitochondrial function controls T cell differentiation, we assessed the ability of *Tfam*-deficient T cells to differentiate into effector T cell subsets. The balance among different functional effector T cell subsets determines the outcome of the immune response and is essential to prevent undesired inflammation and autoimmune diseases. Naive CD4⁺ T cells were labeled with Cell Violet; differentiated in vitro with different cytokines and neutralizing antibodies to Th1, Th2, Th17, and regulatory (Treg) T cell subsets; and assessed for proliferation and expression of transcription factors and cytokines. *Tfam* deficiency greatly impaired proliferation in all the skewing conditions (Figures 6A and 6C). *Tfam*-depleted cells showed higher expression of the Th1-specific transcription T-bet, higher numbers of IFN- γ -producing cells, and higher levels of IFN- γ secretion (Figures 6A, 6B, and 6E). In all polarization conditions, *Tfam*^{-/-} CD4⁺ T cells secreted less IL-4 than WT cells (Figure 6E), demonstrating a Th1/Th2 imbalance toward the Th1 response in the absence of *Tfam*.

When polarized toward Th17 T cell subsets, no substantial differences were found in the number of ROR γ t-expressing cells between *Tfam*^{-/-} and WT cells (Figure 6C). However, impaired mitochondrial function in *Tfam*^{-/-} CD4⁺ T cells significantly reduced the levels of IL-17-producing cells and impaired IL-17 and IL-10 secretion (Figures 6D and 6F), while increasing IFN- γ secretion (Figure 6E). In Treg conditions, no significant differences were found in the number of Foxp3-expressing cells, but *Tfam*^{-/-} CD4⁺ T cells secreted reduced amounts of anti-inflammatory cytokine IL-10 (Figures 6D and 6F). Thus, *Tfam* deficiency favored the appearance of Th17 cells which coexpress ROR γ t and T-bet, and produce high levels of IFN- γ but reduced amounts of IL-10, and which have been proposed to be pathogenic Th17 cells involved in autoimmune diseases in mice (Peters et al., 2011). Collectively, these results reveal a role for mitochondrial function in the regulation of T cell differentiation and indicate that mitochondrial dysfunction is associated with a deregulation of T cell differentiation toward proinflammatory Th1 cell subsets.

Increasing Intracellular NAD⁺ Content Boosts Lysosomal Function and Dampens Th1 Responses in Respiration-Impaired Cells

We then investigated whether lysosomal dysfunction caused by mitochondrial respiration deficiency is involved in the increased inflammatory responses observed in *Tfam*-deficient cells. Naive CD4⁺ T cells activated in the presence of the lysosomal inhibitor leupeptin or SM showed increased levels of IFN- γ mRNA (Figure S5A), suggesting that the lysosomal dysfunction might contribute to the increased proinflammatory profile of *Tfam*^{-/-} CD4⁺ T cells. To ascertain the involvement of lysosome function in the regulation of T cell responses, we studied T cell activation and differentiation in mice lacking ASM, which mimics the LSD Niemann-Pick disease type A (NPA) and, similarly to *Tfam*^{-/-}, shows SM accumulation, lysosomal disorder, and autophagy impairment (Gabandé-Rodríguez et al., 2014). Naive CD4⁺ T cells from *ASM*^{-/-} mice activated in nonskewing conditions showed a higher frequency of IFN- γ -producing cells and higher levels of IFN- γ secretion than WT (Figure 7A). Similarly to respiration-impaired *Tfam*^{-/-} cells, *ASM*^{-/-} cells showed higher frequency of IFN- γ -producing cells in Th1 conditions, and reduced frequency of IL-17-producing cells in Th17 skewing conditions (Figure 7B). T cells from *ASM*^{-/-} mice did not show appreciable mitochondrial alterations in terms of mitochondrial mass, mROS, ATP production, and OCR (Figures S5B–S5D). Collectively, these results show that lysosome dysfunction is sufficient to deregulate T cell differentiation toward proinflammatory Th1 subsets.

Increasing intracellular levels of NAD⁺ has been proposed to be a therapeutic strategy to restore mitochondrial function in respiratory-chain deficiencies (Cerutti et al., 2014; Gomes et al., 2013; Karamanlidis et al., 2013). To assess whether modulation of the cellular NAD⁺/NADH ratio may be involved in the regulation of lysosomal function, we treated *Tfam*-deficient T cells with the nicotinamide precursor NAM to reestablish NAD⁺/NADH balance, and assessed parameters of lysosome function. Addition of NAM increased ASM activity, reduced p62 accumulation, and downregulated TFEB target genes in *Tfam*-deficient cells (Figures 7C–7E), suggesting that modulation

of mitochondrial NAD⁺/NADH levels impacts lysosome function. Finally, to determine whether restoring NAD⁺/NADH levels would limit the increased proinflammatory profile in respiration-impaired *Tfam*^{-/-} T cells, naive CD4⁺ T cells were activated in the presence of NAM for 72 hr and their cytokine profile assessed. NAM treatment reduced the frequency of IFN- γ -producing *Tfam*^{-/-} T cells (Figure S5E). Additionally, under Th1 polarization conditions, naive *Tfam*^{-/-} CD4⁺ T cells cultured in the presence of NAM showed a reduced percentage of IFN- γ -producing cells (Figure 7F), indicating that improved lysosomal function reduces the exacerbated inflammatory response of mitochondrial respiration-impaired cells.

DISCUSSION

Our findings reveal a mechanism through which mitochondrial respiration preserves cellular homeostasis by regulating the function of the endolysosomal compartment during essential biological processes, illustrated here in the regulation of T cell function. We show that lack of *Tfam* in T cells decreases cellular mtDNA content, alters mitochondrial metabolism, and is associated with impaired endolysosomal function, abnormal accumulation of SMs, and increased proinflammatory T cell responses (Figure 7G).

We provide here evidence for primary mitochondrial dysfunction leading to altered lysosomal function and sphingolipidosis. Cells lacking *Tfam* exhibit abnormal lipid trafficking, altered lysosomal Ca²⁺ mobilization, and autophagosome-lysosome fusion defects similar to those seen in LSDs. In Niemann-Pick (NP) type A and B diseases (NPA and NPB), SM accumulates in lysosomes due to insufficient activity of ASM. SM accumulation has been found to inhibit the main calcium channel in the lysosome, impairing endolysosomal trafficking, protein degradation, and macroautophagy (Gabandé-Rodríguez et al., 2014; Shen et al., 2012). Our findings demonstrate that mitochondrial dysfunction results in autophagosome-lysosome fusion defects and reduced mitochondrial clearance by mitophagy, which are commonly observed in almost all sphingolipidoses (Lieberman et al., 2012). A predominant nuclear localization of TFEB has been detected in cells from mouse models of LSD (Sardiello et al., 2009). Mitochondrial respiration deficiency increases TFEB activation, suggesting that the TFEB pathway is activated as a cellular response to lysosomal stress after intralysosomal storage of nondegraded molecules.

Lysosomal calcium level is impaired not only by *Tfam* deletion, which triggers a general lowering of the levels of mtDNA, but also in cells from patients with point mutations in mitochondrial respiratory complex I (CI). Mitochondrial CI is essential for maintenance of the NAD⁺/NADH ratio through NADH dehydrogenase activity, and an imbalanced NAD⁺/NADH ratio in cancer cells with mutations in CI subunits is associated with impaired autophagy and p62 degradation (Santidrian et al., 2013). Inhibition of CI activity with rotenone in a mouse model of Parkinson's disease impairs autophagic flux and promotes p62 and α -synuclein accumulation (Wu et al., 2015). Our data demonstrate that NAD⁺ precursors restore ASM activity, prevent p62 accumulation, and downregulate TFEB target genes in *Tfam*-deficient cells, thus supporting a role of mitochondrial CI and NAD⁺/NADH ratio in the regulation of lysosomal function. These data support the

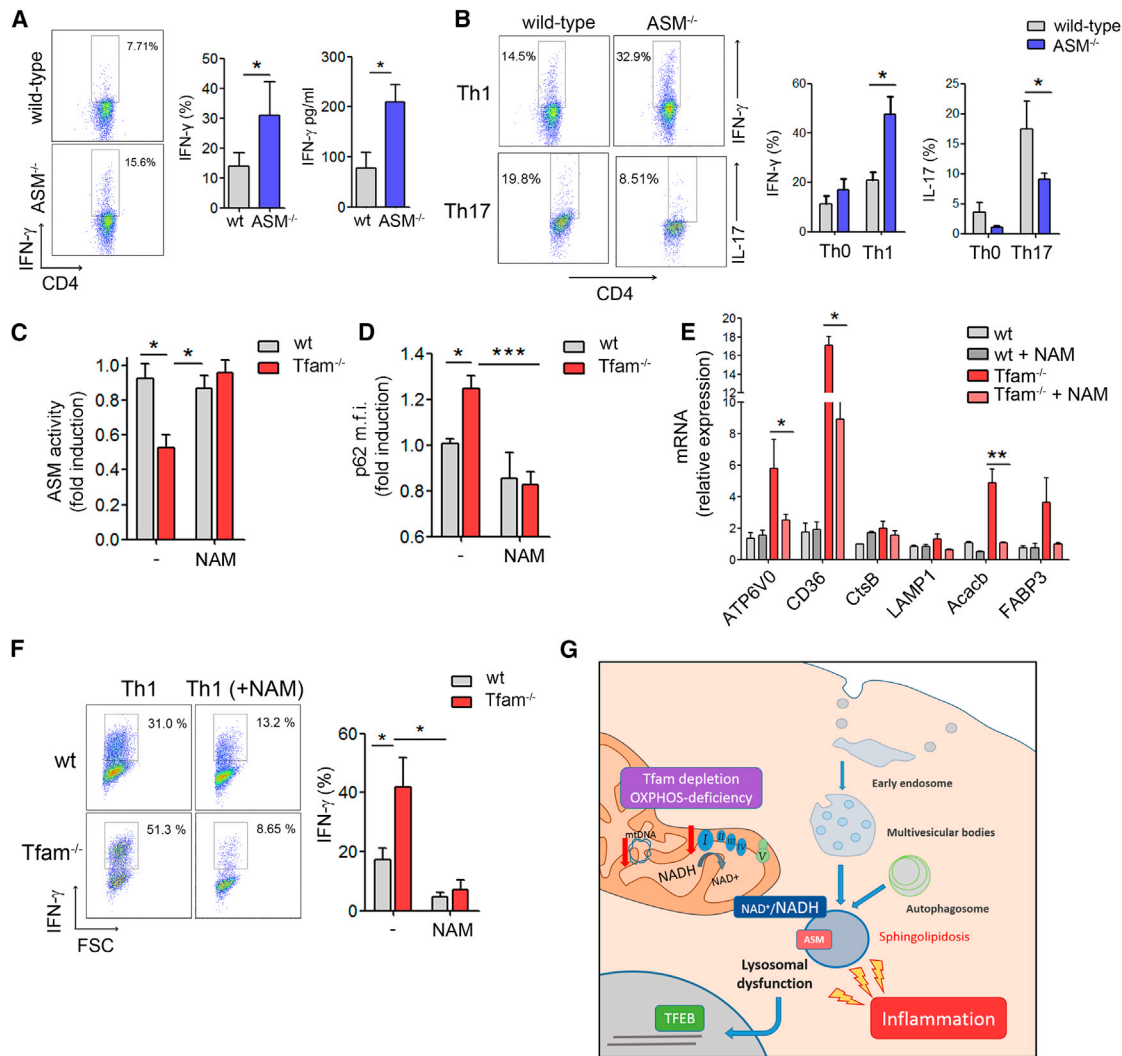


Figure 7. Increasing NAD⁺ Levels Improves Lysosome Function and Reduces Inflammatory Responses in *Tfam*-Deficient Cells

(A) Dot plots show intracellular IFN- γ levels by flow cytometry in CD4 T cells activated with CD3/CD28 (6 days). Graphs show percentage of IFN- γ -producing cells and IFN- γ levels in the supernatant by ELISA.
 (B) CD4 T lymphocytes cultured under Th0, Th1, and Th17 condition for 6 days. Flow cytometry analysis of the frequency of CD4 T cells producing IFN- γ and IL-17.
 (C and D) (C) ASM activity and (D) flow cytometry analysis of p62 levels in T-lymphoblasts treated with NAM (10mM) for 2 days.
 (E) Relative mRNA levels of TFEB target genes in T cells incubated or not with NAM.
 (F) CD4 T cells cultured toward Th1 in the presence or absence of NAM for 3 days. Flow cytometry analysis of the frequency of CD4 T cells producing IFN- γ .
 (G) Diagram representing the proposed mechanism. Data are means \pm SEM (n \geq 3); *p < 0.05, **p < 0.01 and ***p < 0.001 (Student's t test).

notion that lysosomes adapt their biogenesis and function to the metabolic state of the cell by sensing intracellular NAD⁺/NADH levels. Further research is necessary to understand how NAD precursors reestablish ASM activity and control lysosomal function, and whether it relies on transcriptional regulation by sirtuins, NAD-dependent deacetylases.

Recent studies support the contribution of lysosomal homeostasis to the regulation of T cell function during adaptive immune responses (Valdor et al., 2014). The lysosomal dysfunction and elevated SM levels in *Tfam*-deficient cells might be responsible for the acquisition of a proinflammatory profile, since similar cytokine profile was found in *ASM*^{-/-} T cells, which presented

lysosomal dysfunction without altered mitochondrial respiration. Together, our results indicate that loss of lysosomal homeostasis by a primary mitochondrial dysfunction triggers proinflammatory T cell responses. Lysosomal function could regulate immune response by modulating cellular metabolism. By degrading key glycolytic enzymes, lysosome function regulates glycolysis and the production of effector cytokines, including IFN- γ and IL-1 β (Lu et al., 2014).

Our results shed light on how metabolic reprogramming toward anaerobic glycolysis and the alterations to the endolysosomal compartment affect T cell differentiation to effector lineages. It has been reported that Th1, Th2, and Th17 lineages display a

strong bias toward glycolysis over mitochondrial metabolism, whereas Treg cells have a mixed metabolism involving glycolysis, lipid oxidation, and OXPHOS (Gerriets et al., 2015; Michalek et al., 2011). Metabolic reprogramming toward glycolysis in *Tfam*^{-/-} T cells could contribute to their proinflammatory phenotype, since glycolysis enhances IFN- γ expression by preventing GAPDH from its binding to the 3'UTR of IFN- γ mRNA (Chang et al., 2013). Glycolysis is important in driving Th17 differentiation through Hif-1 α (Pearce et al., 2013). In addition, impaired mitochondrial respiration induces succinate accumulation, which impairs prolyl hydroxylase activity, stabilizing Hif-1 α and enhancing IL-1 β production (Tannahill et al., 2013). *Tfam* depletion favors the differentiation of Th1 subsets, dampens Th2 differentiation, and inhibits Th17 T cell subsets. Interestingly, in Th17-skewing conditions, *Tfam*-deficient cells showed reduced IL-17 and IL-10 but increased IFN- γ secretion, which suggests that cues from mitochondria can modulate the differentiation toward pathogenic Th17 cells.

Defects in mitochondrial homeostasis are closely linked to the development of human pathologies such as cancer, inflammation, neurodegenerative diseases, and metabolic disorders (Taylor and Turnbull, 2005), and are also a recurrent hallmark of aging (López-Otín et al., 2013). In summary, our findings on the role of mitochondrial respiration as a regulator of endolysosomal function could therefore provide potential insights into the involvement of mitochondria in human diseases and aging. These findings provide evidence for a functional link between mitochondrial respiration and the endolysosomal system, with implications for treating mitochondrial-related diseases.

EXPERIMENTAL PROCEDURES

Mice, Antibodies, and Reagents

All animal experiments were performed in the specific pathogen-free facilities at CNIC in accordance with European Union recommendations and institutional guidelines. *Tfam*^{fl/fl} mice were kindly provided by N.G. Larsson (Larsson et al., 1998), and CD4Cre^{+/-} mice were purchased from the Jackson Laboratory. Double heterozygotes (*Tfam*^{+/-}, CD4Cre^{+/-}) were obtained and backcrossed to the *Tfam*^{fl/fl} strain to generate tissue-specific knockouts (CD4Cre^{+/-} *Tfam*^{fl/fl}). *ASM*^{-/-} mice were kindly donated by E.H. Schuchman (Mount Sinai School of Medicine, New York). Sources of chemical and biological reagents detailed in Supplemental Experimental Procedures.

Cells, Plasmids, and Cell Transfection

Naive CD4⁺ T cells were obtained by negative selection using the auto-MACS Pro Separator (Miltenyi Biotec). Where stated, cells were activated by stimulation on plates coated with anti-CD3 (5 μ g ml⁻¹) and soluble anti-CD28 (2 μ g ml⁻¹). To obtain differentiated T lymphoblasts, naive CD4⁺ cells were cultured for 36–48 hr with 2 μ g ml⁻¹ concanavalin A, and 50 U ml⁻¹ IL-2 was added every 2 days. Balb/cJ and mt-ND6 (FG23-1) mutant cell line were described (Acín-Pérez et al., 2014). Human fibroblasts from a control, a patient with a point mutation in mt-ND5 gene (m.13513G>A), and a patient with a point mutation in mt-tRNA^{Asn} gene (m.5658T>C) were obtained from skin biopsies for research purposes after written consent in accordance with the Helsinki declaration. The human Jurkat T and the oligodendroglia Oli-Neu cell lines were silenced by lentiviral infection as detailed in Supplemental Experimental Procedures.

T Cell Differentiation, Proliferation, and Intracellular Staining

Naive CD4⁺ CD25⁻ T lymphocytes were obtained from cell suspensions prepared from spleen and peripheral lymph nodes (LN) of *Tfam*^{fl/fl} (wild-type) and CD4⁺Cre^{+/-} *Tfam*^{fl/fl} (*Tfam*^{-/-}) mice. Pooled spleen and LN cells were incubated with biotinylated antibodies to IgM, B220, CD19, CD8, Gr-1, CD44, CD25, MHC-II, F4/8, CD11c, CD11b, and DX5 (BD Pharmingen) followed by

negative selection using the auto-MACS Pro Separator (Miltenyi Biotec). For in vitro activation, naive CD4⁺ T cells were incubated in the presence of 5 μ g ml⁻¹ plastic-bound purified anti-CD3, 2 μ g ml⁻¹ soluble anti-CD28, and 100 U ml⁻¹ human IL-2. For Th0 conditions, anti-IFN- γ (4 μ g ml⁻¹) and IL-4 (4 μ g ml⁻¹) were added. For Th1 conditions, culture was supplemented with IL-12 (10 ng ml⁻¹) and anti-IL-4 (4 μ g ml⁻¹). For Th2 conditions, IL-4 (10 ng ml⁻¹) and anti-IFN- γ (10 μ g ml⁻¹) were added. For Th17 conditions, anti-IL-2 (10 μ g ml⁻¹), anti-IL-4 (10 μ g ml⁻¹), anti-IFN- γ (10 μ g ml⁻¹), TGF- β (5 ng ml⁻¹), IL-23 (20 ng ml⁻¹), and IL-6 (20 ng ml⁻¹) were included in cultures. For Treg cell differentiation, TGF- β (10 ng ml⁻¹) was added. For proliferation assays, cells were labeled with Cell Violet (1 μ M). For intracellular staining of transcription factors, cells were differentiated for 3 days, fixed, permeabilized, and stained with anti-ROR γ T and anti-T-bet (BD Biosciences). For intracellular cytokine staining, cells were restimulated for 4 hr with PMA and ionomycin in the presence of brefeldin, fixed, permeabilized, and stained with anti-CD4, anti-IFN- γ , anti-IL-17, and anti-Foxp3. Data were acquired on a FACSCanto flow cytometer (BD Biosciences) and analyzed with FLOWJO software (Tree Star).

Quantitative Real-Time PCR and mtDNA Analysis

Total RNA was extracted from cells using the RNeasy kit (QIAGEN), and cDNA was synthesized with the High-Capacity cDNA Reverse Transcription Kit (Applied Biosystems). Triplicate reactions were run on a 7500 Fast Real-Time PCR System (Applied Biosystems) using SYBR Green PCR reagents (Applied Biosystems). Data were normalized to the expression of β -actin and β -2-microglobulin and analyzed using Biogazelle QBasePlus software (Biogazelle). For analysis of mtDNA levels, total DNA was extracted with the DNeasy kit (QIAGEN), amplified using primers specific for cytochrome c oxidase subunit 1 (mtCO1) and NADH dehydrogenase 1 (mtND1), and normalized to succinate dehydrogenase (SDH) nuclear gene.

Survival Assays

T lymphoblasts were cultured in RPMI 1640 containing glucose or in RPMI 1640 deprived of glucose (Life Technologies) supplemented with 5 mM galactose and dialyzed FBS. Viable cells were analyzed by HOECHST58 exclusion by flow cytometry.

Mitochondrial Content and ROS

Mitochondrial mass and mitochondrial-derived ROS levels were measured by flow cytometry after labeling cells with Mitotracker green (50 nM) or MitoSOX (2.5 μ M).

Extracellular Flux Analysis and Metabolic Assays

OCRs and extracellular acidification rates (ECAR) were measured in a XF-96 Extracellular Flux Analyzers (Seahorse Bioscience) in cells suspended in XF medium (nonbuffered RPMI 1640 containing either 25 mM glucose or 1 mM palmitate, 2 mM L-glutamine, and 1 mM sodium pyruvate). Three measurements were obtained under basal conditions and upon addition of oligomycin (1 μ M), fluoro-carbonyl cyanide phenylhydrazone (FCCP; 1.5 μ M), and rotenone (100 nM) + antimycin A (1 μ M).

Lysosomal Calcium Mobilization, Content, pH, and Activities

Lysosomal calcium was measured in cells loaded with INDO-1 (2 μ M), and fluorescence intensity ratio at 340/380 nm was detected by flow cytometry. After basal recording, cells were treated with bafilomycin-A1 (1 μ M, Sigma) to promote lysosomal calcium release for the indicated times. Lysosomal content was determined by flow cytometry after incubation with LysoTracker. Lysosomal pH was determined by dual-excitation and dual-emission measurements by flow cytometry with the ratiometric lysosomal pH probe LysoSensor Yellow/Blue DND-160 (Life Technologies, 2 μ M). For analysis of Cathepsin B activity, cells were incubated 30 min with Magic Red (Immunochemistry Technologies) and measured by flow cytometry. Acid phosphatase activity (Sigma) and ASM activity (AAT Bioquest) were performed in total cell lysates following manufacturer's instructions.

Blue Native Gel Electrophoresis, Mitochondrial Complex Activities, and Mitochondrial Membrane Potential Assays

For supercomplex assembly, T lymphocytes were lysed in the presence of digitonin and proteins separated on 5%–13% gradient blue native gels

(Acín-Pérez et al., 2014). Total ATP and mitochondrial-derived ATP synthesis in T cell lysates was measured by kinetic luminescence assay, and activities of individual complexes were measured spectrophotometrically as described (Acín-Pérez et al., 2014). For mitochondrial potential assays, cells were labeled with tetramethylrhodamine methyl ester (TMRM, 100 nM) and analyzed by flow cytometry upon incubation with oligomycin (200 nM) for the indicated times.

Confocal Microscopy Analysis of Autophagy and Mitophagy

Oli-Neu cells were transfected using Lipofectamine (Invitrogen) with LC3-GFP-RFP, and treated or not with Rapamycin (200 nM, Sigma) for 3 hr. For mitophagy assays, Oli-Neu cells transfected with Parkin-GFP were treated or not with CCCP (2 μ M) for 3 hr. Cells were examined with a Leica SP5 confocal microscope (Leica) and analyzed with ImageJ software (NIH).

DSS-Induced Colitis Model

Colitis was induced by daily administration of 3% Dextran Sodium Sulfate (DSS, Mw 30,000–40,000) for 7 days in drinking water. The clinical parameters used to score the disease were weight loss, loose stools/diarrhea, and presence of occult/gross bleeding. At the end of treatment, colons were processed for histological analysis, and mesenteric lymph nodes were processed to study cytokine production of immune cells by flow cytometry.

Statistical Analyses

All values were expressed as the mean \pm SEM. For in vitro experiments, statistical analyses were calculated with Student's *t* test; for in vivo experiments, differences between groups were calculated using the Mann-Whitney U test for unpaired data (GraphPad Prism). Differences were considered significant when **p* \leq 0.05, ***p* \leq 0.01, ****p* \leq 0.001.

SUPPLEMENTAL INFORMATION

Supplemental Information includes five figures and Supplemental Experimental Procedures and can be found with this article at <http://dx.doi.org/10.1016/j.cmet.2015.07.020>.

AUTHOR CONTRIBUTIONS

F.B., R.A.-P., C.V.-B., C.M., N.N.-A., and M.M. performed experimental work. A.B., M.A.M., J.M.R., J.M.F.-P., J.A.E., E.G.-R., and M.D.L. provided materials. F.B., J.A.E., and M.M. designed research. F.B. and M.M. analyzed data and wrote the manuscript.

ACKNOWLEDGMENTS

We thank N.G. Larsson (Max Planck Institute for Biology of Ageing) for *Tfam*^{fl/fl} mice, F. Sanchez-Madrid for support and advice, C. López-Otín and M. Navarro for the critical reading of the manuscript, and S. Bartlett for English editing. F.B. is supported by ERC-2011-AdG 294340-GENTRIS. This work was supported by SAF2011-25834 from Ministerio de Economía y Competitividad-Spain, COST-Action BN1202, Cardiovascular Network RD12-0042-0056 (Instituto de Salud Carlos III). M.M. is supported by Contrato de Investigadores SNS Miguel Servet I (CP14/00219 and MS14/00219) from the Instituto de Salud Carlos III. The Centro Nacional de Investigaciones Cardiovasculares (CNIC, Spain) is supported by the Spanish Ministry of Science and Innovation and the Pro-CNIC Foundation.

Received: October 27, 2014

Revised: April 10, 2015

Accepted: July 22, 2015

Published: August 20, 2015

REFERENCES

Acín-Pérez, R., Carrascoso, I., Baixauli, F., Roche-Molina, M., Latorre-Pellicer, A., Fernández-Silva, P., Mittelbrunn, M., Sanchez-Madrid, F., Pérez-Martos, A., Lowell, C.A., et al. (2014). ROS-triggered phosphorylation of complex II by Fgr kinase regulates cellular adaptation to fuel use. *Cell Metab.* *19*, 1020–1033.

Appleby, R.D., Porteous, W.K., Hughes, G., James, A.M., Shannon, D., Wei, Y.-H., and Murphy, M.P. (1999). Quantitation and origin of the mitochondrial membrane potential in human cells lacking mitochondrial DNA. *Eur. J. Biochem.* *262*, 108–116.

Arruda, A.P., Pers, B.M., Parlakgöl, G., Güney, E., Inouye, K., and Hotamisligil, G.S. (2014). Chronic enrichment of hepatic endoplasmic reticulum-mitochondria contact leads to mitochondrial dysfunction in obesity. *Nat. Med.* *20*, 1427–1435.

Buchet, K., and Godinot, C. (1998). Functional F1-ATPase essential in maintaining growth and membrane potential of human mitochondrial DNA-depleted rho⁰ cells. *J. Biol. Chem.* *273*, 22983–22989.

Cerutti, R., Pirinen, E., Lamperti, C., Marchet, S., Sauve, A.A., Li, W., Leoni, V., Schon, E.A., Dantzer, F., Auwerx, J., et al. (2014). NAD(+)-dependent activation of Sirt1 corrects the phenotype in a mouse model of mitochondrial disease. *Cell Metab.* *19*, 1042–1049.

Chang, C.H., Curtis, J.D., Maggi, L.B., Jr., Faubert, B., Villarino, A.V., O'Sullivan, D., Huang, S.C., van der Windt, G.J., Blagih, J., Qiu, J., et al. (2013). Posttranscriptional control of T cell effector function by aerobic glycolysis. *Cell* *153*, 1239–1251.

Daniele, T., Hurbain, I., Vago, R., Casari, G., Raposo, G., Tacchetti, C., and Schiaffino, M.V. (2014). Mitochondria and melanosomes establish physical contacts modulated by Mfn2 and involved in organelle biogenesis. *Curr. Biol.* *24*, 393–403.

Detmer, S.A., and Chan, D.C. (2007). Functions and dysfunctions of mitochondrial dynamics. *Nat. Rev. Mol. Cell Biol.* *8*, 870–879.

Ekstrand, M.I., Falkenberg, M., Rantanen, A., Park, C.B., Gaspari, M., Hultenby, K., Rustin, P., Gustafsson, C.M., and Larsson, N.G. (2004). Mitochondrial transcription factor A regulates mtDNA copy number in mammals. *Hum. Mol. Genet.* *13*, 935–944.

Elbaz-Alon, Y., Rosenfeld-Gur, E., Shinder, V., Futerman, A.H., Geiger, T., and Schuldiner, M. (2014). A dynamic interface between vacuoles and mitochondria in yeast. *Dev. Cell* *30*, 95–102.

Friedman, J.R., and Nunnari, J. (2014). Mitochondrial form and function. *Nature* *505*, 335–343.

Futerman, A.H., and van Meer, G. (2004). The cell biology of lysosomal storage disorders. *Nat. Rev. Mol. Cell Biol.* *5*, 554–565.

Gabandé-Rodríguez, E., Boya, P., Labrador, V., Dotti, C.G., and Ledesma, M.D. (2014). High sphingomyelin levels induce lysosomal damage and autophagy dysfunction in Niemann Pick disease type A. *Cell Death Differ.* *21*, 864–875.

Gerriets, V.A., Kishton, R.J., Nichols, A.G., Macintyre, A.N., Inoue, M., Ilkayeva, O., Winter, P.S., Liu, X., Priyadharshini, B., Slawinska, M.E., et al. (2015). Metabolic programming and PDHK1 control CD4+ T cell subsets and inflammation. *J. Clin. Invest.* *125*, 194–207.

Gomes, A.P., Price, N.L., Ling, A.J., Moslehi, J.J., Montgomery, M.K., Rajman, L., White, J.P., Teodoro, J.S., Wrann, C.D., Hubbard, B.P., et al. (2013). Declining NAD(+) induces a pseudohypoxic state disrupting nuclear-mitochondrial communication during aging. *Cell* *155*, 1624–1638.

Hönscher, C., Mari, M., Auffarth, K., Bohnert, M., Griffith, J., Geerts, W., van der Laan, M., Cabrera, M., Reggiori, F., and Ungermann, C. (2014). Cellular metabolism regulates contact sites between vacuoles and mitochondria. *Dev. Cell* *30*, 86–94.

Houtkooper, R.H., Mouchiroud, L., Ryu, D., Moullan, N., Katsyuba, E., Knott, G., Williams, R.W., and Auwerx, J. (2013). Mitonuclear protein imbalance as a conserved longevity mechanism. *Nature* *497*, 451–457.

Karamanlidis, G., Lee, C.F., Garcia-Menendez, L., Kolwicz, S.C., Jr., Suthamarak, W., Gong, G., Sedensky, M.M., Morgan, P.G., Wang, W., and Tian, R. (2013). Mitochondrial complex I deficiency increases protein acetylation and accelerates heart failure. *Cell Metab.* *18*, 239–250.

Lapiente-Brun, E., Moreno-Loshuertos, R., Acín-Pérez, R., Latorre-Pellicer, A., Colás, C., Balsa, E., Perales-Clemente, E., Quirós, P.M., Calvo, E., Rodríguez-Hernández, M.A., et al. (2013). Supercomplex assembly determines electron flux in the mitochondrial electron transport chain. *Science* *340*, 1567–1570.

- Larsson, N.G., Wang, J., Wilhelmsson, H., Oldfors, A., Rustin, P., Lewandoski, M., Barsh, G.S., and Clayton, D.A. (1998). Mitochondrial transcription factor A is necessary for mtDNA maintenance and embryogenesis in mice. *Nat. Genet.* **18**, 231–236.
- Lieberman, A.P., Puertollano, R., Raben, N., Slaugenhaupt, S., Walkley, S.U., and Ballabio, A. (2012). Autophagy in lysosomal storage disorders. *Autophagy* **8**, 719–730.
- Lloyd-Evans, E., Morgan, A.J., He, X., Smith, D.A., Elliot-Smith, E., Sillence, D.J., Churchill, G.C., Schuchman, E.H., Galione, A., and Platt, F.M. (2008). Niemann-Pick disease type C1 is a sphingosine storage disease that causes deregulation of lysosomal calcium. *Nat. Med.* **14**, 1247–1255.
- López-Otin, C., Blasco, M.A., Partridge, L., Serrano, M., and Kroemer, G. (2013). The hallmarks of aging. *Cell* **153**, 1194–1217.
- Lu, W., Zhang, Y., McDonald, D.O., Jing, H., Carroll, B., Robertson, N., Zhang, Q., Griffin, H., Sanderson, S., Lakey, J.H., et al. (2014). Dual proteolytic pathways govern glycolysis and immune competence. *Cell* **159**, 1578–1590.
- Medina, D.L., Di Paola, S., Peluso, I., Armani, A., De Stefani, D., Venditti, R., Montefusco, S., Scotto-Rosato, A., Prezioso, C., Forrester, A., et al. (2015). Lysosomal calcium signalling regulates autophagy through calcineurin and TFEB. *Nat. Cell Biol.* **17**, 288–299.
- Michalek, R.D., Gerriets, V.A., Jacobs, S.R., Macintyre, A.N., MacIver, N.J., Mason, E.F., Sullivan, S.A., Nichols, A.G., and Rathmell, J.C. (2011). Cutting edge: distinct glycolytic and lipid oxidative metabolic programs are essential for effector and regulatory CD4⁺ T cell subsets. *J. Immunol.* **186**, 3299–3303.
- Osellame, L.D., Rahim, A.A., Hargreaves, I.P., Gegg, M.E., Richard-Londt, A., Brandner, S., Waddington, S.N., Schapira, A.H., and Duchon, M.R. (2013). Mitochondria and quality control defects in a mouse model of Gaucher disease—links to Parkinson's disease. *Cell Metab.* **17**, 941–953.
- Pearce, E.L., Poffenberger, M.C., Chang, C.H., and Jones, R.G. (2013). Fueling immunity: insights into metabolism and lymphocyte function. *Science* **342**, 1242–1245.
- Peters, A., Lee, Y., and Kuchroo, V.K. (2011). The many faces of Th17 cells. *Curr. Opin. Immunol.* **23**, 702–706.
- Rowland, A.A., and Voeltz, G.K. (2012). Endoplasmic reticulum-mitochondria contacts: function of the junction. *Nat. Rev. Mol. Cell Biol.* **13**, 607–625.
- Santidrian, A.F., Matsuno-Yagi, A., Rittland, M., Seo, B.B., LeBoeuf, S.E., Gay, L.J., Yagi, T., and Felding-Habermann, B. (2013). Mitochondrial complex I activity and NAD⁺/NADH balance regulate breast cancer progression. *J. Clin. Invest.* **123**, 1068–1081.
- Sardiello, M., Palmieri, M., di Ronza, A., Medina, D.L., Valenza, M., Gennarino, V.A., Di Malta, C., Donaudy, F., Embrione, V., Polishchuk, R.S., et al. (2009). A gene network regulating lysosomal biogenesis and function. *Science* **325**, 473–477.
- Settembre, C., De Cegli, R., Mansueto, G., Saha, P.K., Vetrini, F., Visvikis, O., Huynh, T., Carissimo, A., Palmer, D., Klisch, T.J., et al. (2013a). TFEB controls cellular lipid metabolism through a starvation-induced autoregulatory loop. *Nat. Cell Biol.* **15**, 647–658.
- Settembre, C., Fraldi, A., Medina, D.L., and Ballabio, A. (2013b). Signals from the lysosome: a control centre for cellular clearance and energy metabolism. *Nat. Rev. Mol. Cell Biol.* **14**, 283–296.
- Shen, D., Wang, X., Li, X., Zhang, X., Yao, Z., Dibble, S., Dong, X.P., Yu, T., Lieberman, A.P., Showalter, H.D., and Xu, H. (2012). Lipid storage disorders block lysosomal trafficking by inhibiting a TRP channel and lysosomal calcium release. *Nat. Commun.* **3**, 731.
- Tannahill, G.M., Curtis, A.M., Adamik, J., Palsson-McDermott, E.M., McGettrick, A.F., Goel, G., Frezza, C., Bernard, N.J., Kelly, B., Foley, N.H., et al. (2013). Succinate is an inflammatory signal that induces IL-1 β through HIF-1 α . *Nature* **496**, 238–242.
- Taylor, R.W., and Turnbull, D.M. (2005). Mitochondrial DNA mutations in human disease. *Nat. Rev. Genet.* **6**, 389–402.
- Valdor, R., Mocholi, E., Botbol, Y., Guerrero-Ros, I., Chandra, D., Koga, H., Gravekamp, C., Cuervo, A.M., and Macian, F. (2014). Chaperone-mediated autophagy regulates T cell responses through targeted degradation of negative regulators of T cell activation. *Nat. Immunol.* **15**, 1046–1054.
- Vernochet, C., Mourier, A., Bezy, O., Macotela, Y., Boucher, J., Rardin, M.J., An, D., Lee, K.Y., Ilkayeva, O.R., Zingaretti, C.M., et al. (2012). Adipose-specific deletion of TFAM increases mitochondrial oxidation and protects mice against obesity and insulin resistance. *Cell Metab.* **16**, 765–776.
- Viader, A., Sasaki, Y., Kim, S., Strickland, A., Workman, C.S., Yang, K., Gross, R.W., and Milbrandt, J. (2013). Aberrant Schwann cell lipid metabolism linked to mitochondrial deficits leads to axon degeneration and neuropathy. *Neuron* **77**, 886–898.
- Weinberg, S.E., Sena, L.A., and Chandel, N.S. (2015). Mitochondria in the regulation of innate and adaptive immunity. *Immunity* **42**, 406–417.
- Wu, F., Xu, H.D., Guan, J.J., Hou, Y.S., Gu, J.H., Zhen, X.C., and Qin, Z.H. (2015). Rotenone impairs autophagic flux and lysosomal functions in Parkinson's disease. *Neuroscience* **284**, 900–911.